Channel noise and synchronization in excitable membranes

Gerhard Schmid, Igor Goychuk, Peter Hänggi*

Universität Augsburg, Institut für Physik, Theoretische Physik I, D-86135 Augsburg, Germany

1. Introduction

A fundamental question in neurophysiology concerns the limiting factors of the reliability of neuronal responses to given stimuli. In this article we focus on a particular aspect of this complex issue: the impact of channel noise, which is generated by random gating dynamics of the ion channels in membrane patches of finite size. In particular, we investigate the effect of channel noise on the synchronization between the action potential produced by the cell membrane patch of finite size and the applied periodic stimulus.

* Corresponding author. Tel.: +49-821-598-3250; fax: +49-821-598-3222.
E-mail address: peter.hanggi@physik.uni-augsburg.de (P. Hänggi).

The topic of synchronization, especially in biological systems, attracts ever growing interest, see Refs. [1–4]. Some prominent examples are the collective flashing of fireflies [5], the synchronization between the respiratory and cardiac activity in human cardiorespiratory system [6], and the signal processing in sensory systems [7,8]. Recently, the phenomena of frequency and phase synchronization have been explored in presence of ambient noise sources, both for a noisy (overdamped) relaxation dynamics [3,9,10] and for an oscillatory stochastic dynamics [3,11]. The theoretical research is further inspired by experimental activities, and vice versa. In the context of theoretical modeling, the frequency and phase synchronization [12] has been observed, for example, in the integrate-and-fire model of the excitable dynamics driven by white noise and an externally applied stochastic spike train [13]. For an optimal dose of noise the mean firing rate of the driven neuron becomes locked by the mean frequency of the external spike train.

2. The Hodgkin–Huxley model

Our starting point is the well-established model of Hodgkin and Huxley [14]. The membrane patch of area S is considered as an electrical capacitor possessing the specific area capacitance C. The membrane separates two ionic bath solutions (which in vivo correspond to the interior and the exterior of the excitable cell) with different concentrations of the ions of different sorts, mainly potassium, K^+, sodium, Na^+, and chloride, Cl^- ions. The macroscopic concentration differences are kept approximately constant. In the cell, this task is accomplished by the ATP-driven ionic pumps. Furthermore, the ionic baths are on the average electrically neutral. However, due to the different ionic concentrations on the opposite sides of the semi-permeable membrane, the membrane becomes charged. As a consequence, an equilibrium transmembrane electrical potential difference emerges. The lipid membrane creates an almost impenetrable barrier for the ions. However, they can flow across the membrane through special ion selective pores created by specialized membrane proteins—the ion channels [15]. The specific potassium, I_K, and sodium, I_{Na}, ion currents through the open ion channels are approximately proportional to the differences of the transmembrane potential V and the specific (for the particular sort of ions) equilibrium potentials, E_K and E_{Na}, respectively. The *stochastically* averaged, mean conductances, $G_{Na}(m,h)$ and $G_K(n)$, are, however, strongly nonlinear functions of V. This nonlinearity emerges due to the gating dynamics (see below). There exists also the leakage current I_L, mainly due to the chloride ions. If the membrane is driven by the external current $I_{\mathrm{ext}}(t)$, the sum of the specific ion currents and the capacitive current, I_C, must be equal to $I_{\mathrm{ext}}(t)$ as a consequence of the charge conservation. Therefore, the equation for the transmembrane potential $V(t)$ reads

$$C\,\frac{\mathrm{d}}{\mathrm{d}t}\,V + G_K(n)\;(V - E_K) + G_{Na}(m,h)\;(V - E_{Na}) + G_{\mathrm{L}}\;(V - E_L) = I_{\mathrm{ext}}(t)\;. \tag{1}$$

For a squid giant axon, the parameters in Eq. (1) are $E_{Na} = 50$ mV, $E_K = -77$ mV, $E_L = -54.4$ mV, and $C = 1$ μF/cm^2. Furthermore, the leakage conductance is assumed to be constant, $G_L = 0.3$ mS/cm^2. On the contrary, the sodium and potassium conductances are controlled by the voltage-dependent gating dynamics of single ion channels and are proportional to their respective numbers. These latter assumptions have been fully confirmed in the single-channel recordings by Neher, Sakmann and colleagues which indeed have proven that ion channels undergo the opening-closing stochastic gating dynamics [16]. In the Hodgkin–Huxley model, the opening of the potassium ion channel is governed by four identical activation gates characterized by the opening probability n. The channel is open when all four gates are open. In the case of sodium channel, the dynamics is governed by the three independent, identical fast activation gates (m) and an additional slow, so-termed inactivation gate (h). The independence of the gates implies that the probability $P_{K,Na}$ of the occurrence of the conducting conformation is $P_K = n^4$ for a potassium channel and $P_{Na} = m^3\, h$ for a sodium channel, respectively. In the mean-field description, the macroscopic potassium and sodium conductances thus read:

$$G_K(n) = g_K^{\max}\; n^4, \qquad G_{Na}(m,h) = g_{Na}^{\max}\; m^3 h\;, \tag{2}$$

where $g_K^{\max} = 36$ mS/cm^2 and $g_{Na}^{\max} = 120$ mS/cm^2 denote the maximal conductances (when all channels are open). The two-state, open–closing dynamics of the gates is given by the voltage dependent opening and closing rates $\alpha_x(V)$ and $\beta_x(V)$ ($x = m, h, n$), i.e.,

$$\alpha_m(V) = \frac{0.1(V+40)}{1-\exp[-(V+40)/10]}\;, \tag{3a}$$

$$\beta_m(V) = 4\exp[-(V+65)/18]\;, \tag{3b}$$

$$\alpha_h(V) = 0.07\exp[-(V+65)/20]\;, \tag{3c}$$

$$\beta_h(V) = \{1+\exp[-(V+35)/10]\}^{-1}\;, \tag{3d}$$

$$\alpha_n(V) = \frac{0.01\;(V+55)}{1-\exp[-(V+55)/10]}\;, \tag{3e}$$

$$\beta_n(V) = 0.125\exp[-(V+65)/80]\;. \tag{3f}$$

Hence, the dynamics of the opening probabilities for the gates are given by

$$\dot{x} = \alpha_x(V)\;(1-x) - \beta_x(V)\;x, \qquad x = m,h,n\;. \tag{4}$$

The voltage equation (1), (2), and the rate equations of the gating dynamics (3),(4) define the original, purely deterministic Hodgkin–Huxley model [14] for the squid giant axon. Operating with the average number of open channels, disregards, however, the corresponding number fluctuations (the so-called channel noise [16,17]). Therefore, the Hodgkin–Huxley model is valid, strictly speaking, only within the limit of very large system size where these fluctuations can be neglected. The role of internal fluctuations in membrane patches of finite size cannot, however, be a priori neglected. In fact, the recent theoretical studies make it clear that the channel noise can be functionally important for the excitable dynamics [17–20].

3. Stochastic generalization of Hodgkin–Huxley model

To account for the effect of channel noise, we use the model which presents a stochastic generalization of the Hodgkin–Huxley equations (1)–(4) due to Fox and Lu [21]. The dynamics of the gating variables is given by the following Langevin equation:

$$\dot{x} = \alpha_x(V)\ (1-x) - \beta_x(V)\ x + \xi_x(t), \quad x = m, h, n\ , \tag{5}$$

with independent Gaussian white noise sources $\xi_x(t)$ of vanishing mean which take into account the fluctuations of the number of open gates. The noise strengths depend on the membrane voltage. The noise correlations assume the following form for an excitable membrane patch with N_{Na} sodium and N_K potassium ion channels [21]:

$$\langle \xi_m(t)\xi_m(t')\rangle = \frac{2}{N_{Na}}\,\frac{\alpha_m\beta_m}{(\alpha_m+\beta_m)}\,\delta(t-t')\ , \tag{6a}$$

$$\langle \xi_h(t)\xi_h(t')\rangle = \frac{2}{N_{Na}}\,\frac{\alpha_h\beta_h}{(\alpha_h+\beta_h)}\,\delta(t-t')\ , \tag{6b}$$

$$\langle \xi_n(t)\xi_n(t')\rangle = \frac{2}{N_K}\,\frac{\alpha_n\beta_n}{(\alpha_n+\beta_n)}\,\delta(t-t')\ . \tag{6c}$$

To ensure the confinement of the gating variables between 0 (all gates are closed) and 1 (all gates are open) we implemented numerically the reflecting boundaries at 0 and 1. With the assumption of homogeneous ion channel densities, $\rho_{Na} = 6 \times 10^{13}\ \mathrm{m}^{-2} = 60\ \mu\mathrm{m}^{-2}$ and $\rho_K = 1.8 \times 10^{13}\ \mathrm{m}^{-2} = 18\ \mu\mathrm{m}^{-2}$, the ion channel numbers are given by

$$N_{Na} = \rho_{Na}S, \quad N_K = \rho_K S\ . \tag{7}$$

With decreasing patch size S we observe from our numerical simulations of the Langevin equations (5)–(6) the more and more increasing spiking activity due to the internal channel noise, see Fig. 1.

4. Synchronization in excitable membranes

4.1. Channel noise induced spiking activity: intrinsic coherence resonance

We investigate numerically the influence of channel noise in the absence of external stimulation. For small internal noise strengths, i.e., large patch sizes, the occurrence of action potentials is very rare in the autonomous, nondriven regime: $I_{\mathrm{ext}} = 0$, see Fig. 1. The distribution of interspike intervals $\{T_i := t_{i+1} - t_i\}$ is widely spread with longer intervals becoming less and less probable, see the solid line in Fig. 2(a). With increasing channel noise the firing rate increases as well, and the interspike interval time–histogram depicts a more distinct peak structure, Fig. 2(b). For small membrane patches, the fluctuations of the number of open ion channels dominate the excitable dynamics and after a firing event the membrane patch tends to fire immediately again,

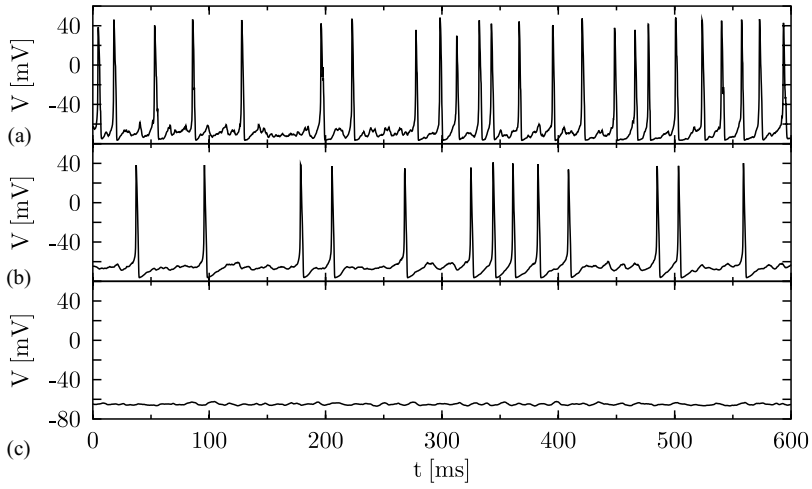

Fig. 1. Three simulated realizations of voltage spike trains for different patch sizes: (a) 1 μm^2, (b) 16 μm^2, and (c) 128 μm^2. With decreasing patch size (bottom-to-top) the fluctuations of the number of open ion channels dominate the dynamics; therefore more action potentials are produced, whereas for very large patch sizes the intrinsic channel noise strength is not capable to produce corresponding voltage spikes.

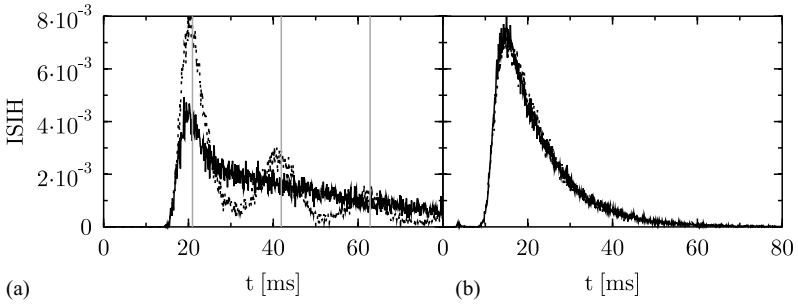

Fig. 2. The interspike interval histograms (ISIH) for the undriven case, $I_{\text{ext}} = 0$, (solid line) and the driven case, $I_{\text{ext}} = \sin(0.3 \cdot t)$, (dotted line) for two patch sizes: (a) 16 μm^2, and (b) 1 μm^2. The driving independent single-peak-structure becomes more and more accentuated for decreasing patch size, i.e., with increasing strength of the channel noise. The refractory period T_r acts as lower bound to the interspike intervals. It varies with the patch area and becomes smaller for smaller patch sizes, cf. $T_r \approx 15$ ms in part (a) vs. $T_r < 10$ms in part (b). The driving–induced peaks appear for sufficiently small internal noise at multiples of the driving period $T_{driving} \approx 21$ ms, cf. part (a). In case of dominating channel noise, the influence of driving on the ISIH is barely distinguishable, cf. part (b).

but after some refractory time which is necessary to achieve the resting potential after hyperpolarization. The above elucidation suggests that with decreasing patch size the spiking activity becomes more regular. A quantity that measures this regularity is the so-called coefficient of variation (CV), or the relative dispersion of the interspike

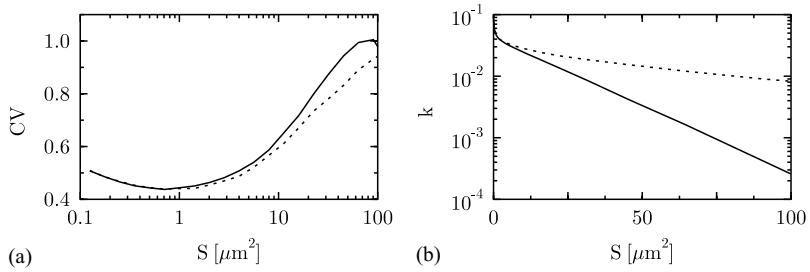

Fig. 3. (a) The dependence of the coefficient of variation CV in (8) versus patch sizes. (b) Firing rates $k = 1/\langle T \rangle$ for the undriven (solid line) and driven case (dotted line, $I_{\text{ext}} = \sin(0.3 \cdot t)$) are depicted versus the patch areas. While the firing rate is monotonically decreasing with increasing patch size the coefficient of variation evidences the phenomenon of intrinsic coherence resonance.

interval distribution, i.e.,

$$CV := \frac{\sqrt{\langle T^2 \rangle - \langle T \rangle^2}}{\langle T \rangle} , \tag{8}$$

which involves the mean interspike interval $\langle T \rangle := \lim_{N\to\infty} \sum(t_{i+1} - t_i)/N$ and the mean squared interval $\langle T^2 \rangle := \lim_{N\to\infty} \sum(t_{i+1} - t_i)^2/N$. For a fully uncorrelated sequence of spikes, which corresponds to the Poissonian spike train, the coefficient of variation would assume the value $CV = 1$. For a more ordered spike train, the coefficient of variation assumes values less then one, $CV < 1$. For a purely deterministic signal, the CV equals to zero.

Fig. 3 depicts the coefficient of variation (8) and the firing rate $k = 1/\langle T \rangle$. While the firing rate decreases monotonically with respect to the patch area, the CV reveals the novel phenomenon of intrinsic coherence resonance [19]. At an optimal dose of internal noise, i.e., an optimal size of the cell membrane patch near $S = 1$ μm^2, the CV exhibits a minimum, where the spike train becomes distinctly more ordered. With decreasing noise level (large S) this feature becomes increasingly diminished, and the CV increases.

4.2. Sub-threshold sinusoidal driving

Next, we switch on an external, *sub-threshold* sinusoidal driving, i.e.,

$$I_{\text{ext}} := A \sin(\Omega t) . \tag{9}$$

with $A < A_{th}$, where A_{th} is the threshold amplitude of driving in the deterministic limit, $S \to \infty$. For $\Omega = 0.3$ ms^{-1} in Fig. 2, $A_{th} \approx 1.6$ μA/cm^2. Interestingly enough the distribution of interspike intervals is not affected much for small patch sizes near $S \approx 1$ μm^2, cf. Fig. 2(b), where the solid and dotted curves are barely distinguishable; see also Fig. 3(a) at $S \approx 1$ μm^2. In this case, the spiking activity possesses an internal

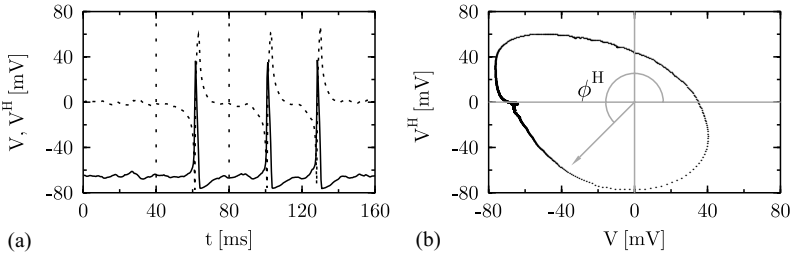

Fig. 4. Stochastic (Hilbert) phase process: (a) realization of the voltage signal (solid line) and the corresponding Hilbert transform (dotted line); (b) The trajectory in $\{V, V^H\}$-space is plotted for the time interval in (a) which is determined by two dashed vertical lines at $t = 40$ ms and $t = 80$ ms, respectively, containing a single firing event. The $\{V(t), V^H(t)\}$-space trajectory undergoes a full 2π-revolution during such a single firing event.

rhythm which withstands the external disturbances. For larger patch sizes the internal noise decreases and the periodic driving induces peaks at multiples of the driving period, see Fig. 2(a). In this regime the external driving imposes a more ordered spiking activity which is characterized by a reduced CV, see Fig. 3(a).

4.3. The concept of stochastic phase processes: frequency synchronization

In order to explore the stochastic phase and stochastic frequency synchronization between the membrane spiking activity and the driving current, one has to invoke the concept of a phase process linked to the stochastic voltage signal $V(t)$. The Hilbert phase $\phi^H(t)$ constitutes one such appropriate phase definition. The corresponding approach is based on the Hilbert transform, it has been originally introduced by Gabor [22,23]. The signal is extended into the complex plane with the imaginary axis given by the Hilbert transform of signal, V^H, cf. Fig. 4:

$$z_V(t) := V(t) + iV^H(t)\,, \tag{10}$$

with

$$V^H(t) = H[V](t) = \frac{1}{\pi} P \int_{-\infty}^{\infty} \frac{V(\tau)}{t-\tau}\,\mathrm{d}\tau\,. \tag{11}$$

The integral in (11) is evaluated in the sense of the Cauchy principal value (P). The Hilbert transform is then used to define the corresponding stochastic process for the Hilbert phase $\phi^H(t)$, i.e.,

$$\phi^H(t) = \arctan\left[\frac{V^H(t)}{V(t)}\right]\,. \tag{12}$$

Here, the phase should be understood as continuously growing function of time. In Fig. 4(a) a realization of the voltage signal and the related Hilbert transform are plotted. Each repeated firing event corresponds to a cycle in the $\{V, V^H\}$–space, see 4(b)); it thus adds an 2π-increment to the phase of the voltage signal. The corresponding Hilbert

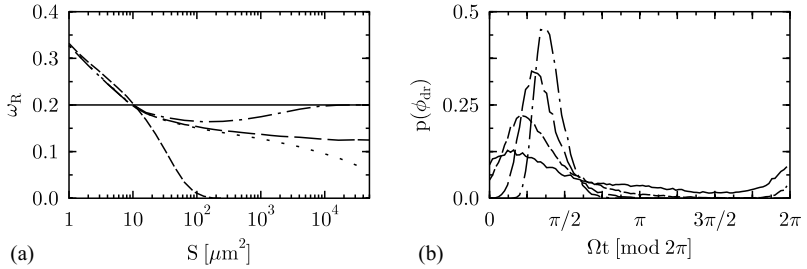

Fig. 5. (a) The dependence of Rice frequency (15) on the patch size is plotted for three sub-threshold amplitudes A of the sinusoidal stimulus $I_{\text{ext}}(t)=A\sin(0.2\cdot t)$: $A=0.0$ μA/cm^2 (short–dashed line), $A=2.02$ μA/cm^2 (dotted line), $A=2.05$ μA/cm^2 (long–dashed line), and for a super-threshold amplitude $A=2.2$ μA/cm^2 (dotted–dashed line). The threshold amplitude is $A_{th}\approx 2.1$ μA/cm^2. The level line displays the angular driving frequency $\Omega=0.2$ ms^{-1}. For subthreshold signals the firing rate vanishes for large areas and the Rice frequency approaches zero, while for a super-threshold amplitude the driving frequency value is attained. (b) The phase probability density $p(\phi_{dr})$ of spiking events versus the phase $\phi_{dr}=\Omega t$ of the driving signal is plotted for $A=2.05$ μA/cm^2 and four different patch areas: $S=4$ μm^2 (solid line); $S=16$ μm^2 (short–dashed line); $S=64$ μm^2 (long–dashed line); $S=256$ μm^2 (dotted–dashed line).

phase frequency ω_H is then given by

$$\omega_H := \lim_{t\to\infty} \frac{\phi^H(t)}{t}\,. \tag{13}$$

An alternative phase definition uses the feature of the point process that is generated by the spikes of the voltage signal $V(t)$. These spikes define marker events at times $\{t_i\}$ with each of them pinpointing the completion of a cycle. The phase increase between two subsequent marker events is then given exactly by 2π. Moreover, by a linear interpolation it is possible to define the instantaneous phase $\phi^R(t)$; i.e.,

$$\phi^R(t) = 2\pi\,\frac{t-t_i}{t_{i+1}-t_i} + 2\pi i \quad (t_i \leqslant t \leqslant t_{i+1})\,, \tag{14}$$

where the times t_i are fixed by the marker events. The average frequency of the process $\phi^R(t)$ is then given by

$$\omega_R = \lim_{t\to\infty} \frac{\phi^R(t)}{t} = 2\,\pi \lim_{t\to\infty} \frac{N(t)}{t}\,, \tag{15}$$

where $N(t)$ denotes the total number of spikes within the time interval $[0,t]$. The index R alludes to the so-called Rice frequency [3,11,24].

Since each action potential adds, on the one hand, the 2π-increment to the Hilbert-phase and, on the other hand, defines the corresponding single marker event, the Hilbert frequency equals the Rice frequency, although the two phase definitions are different.

4.4. Imperfect synchronization for a periodically driven membrane patch

The dependence of the mean frequency ω_R on the patch size is depicted in Fig. 5(a) for driving signals with frequency $\Omega=0.2$ ms^{-1} and for different driving amplitudes A.

In the strong noise regime, the spiking activity is determined by the internal noise and is independent of the driving frequency and amplitude. For intermediate-to-small noise strengths the spike occurrences are locked to *multiples* of the driving period, cf. Fig. 2(a).

This synchronization behavior is also reestablished in the phase probability density $p(\phi_{dr})$ of spiking events in Fig. 5(b). The latter quantity is defined with respect to the phase $\phi_{dr} = \Omega t$ of the driving signal within the driving period, i.e., $0 \leqslant \phi_{dr} < 2\pi$. For small patch sizes, i.e., for a large channel noise, the probability density $p(\phi_{dr})$ is relatively flat. When the channel noise diminishes a peak structure becomes more and more pronounced. It worth to notice that spikes occur most frequently *before* the driving current reaches its maximum at $\Omega t = \pi/2$. The occurrence of the spike thus *forecasts* that the signal's maximum will be reached soon. This effect is similar to the effect of *anticipated synchronization* between master and slave neurons [25]. Moreover, a very interesting new effect is noticeable in Fig. 5(b): the phase lag between the maximum of $p(\phi_{dr})$ and the signal maximum at $\phi_{dr} = \pi/2$ *increases* upon increasing the channel noise strength. In other words, the smaller membrane patch fires most probably more in advance than the larger patch, although the probability distribution of the spikes occurrence is increasingly flattened. This prominent effect can be explained as follows. The increase of noise strength certainly helps to overcome the firing threshold. Therefore, the system tends to fire more and more in advance, before the maximum of signal is reached. However, the noise increases also the uncertainty of firing events and, therefore, the probability distribution becomes flat.

Even though the observed locking behavior presents clearly some sort of synchronization, no *perfect* frequency synchronization—characterized by a perfect locking of the mean frequency (13) to the external driving frequency—can be detected, see Fig. 5(a). While for large, but still sub-threshold stimuli $A < A_{th} \approx 2.1\ \mu\mathrm{A/cm^2}$ a plateau is formed over a wide range of noise strengths, the mean frequency, which corresponds to this plateau, does not match the driving frequency. This frequency mismatch happens due to the multimodal structure of ISIH, which is caused by the locking of the firing occurrences to the external force period in ratios different from 1:1. A similar phenomenon of imperfect synchronization has also been found in the human cardiorespiratory activity [6]. The plateau corresponds to the situation where nearly every maximum of the driving force produces a spike. Nevertheless, some driving maxima produce no spikes and therefore the mean frequency is smaller than the driving frequency. We point out, however, that for a signal represented by a stochastic spike train, like in Ref. [13], a perfect synchronization should be observed. The reason is that a random driving with the mean frequency $\langle\Omega\rangle$ will not produce additional maxima in the ISIH at the multiplies of the *mean* driving frequency. The occurrence of such maxima thereby destroys the perfect synchronization in the periodic case.

The situation changes with a super-threshold stimuli, see dashed–dotted line in Fig. 5(a): here the increasing strength of the channel noise with decreasing size S destroys the perfect frequency synchronization. This is caused by the skipping of some firing events, or by the generation of additional spikes.

5. Conclusions

In conclusion, we have investigated the synchronization in a noisy generalization of the Hodgkin–Huxley model, which incorporates the spontaneous fluctuations of the membrane conductivity due to the individual ion channel dynamics—the so-called channel noise. In the absence of an externally applied stimulus the excitable membrane patch exhibits a noise-induced rhythmic spiking activity at an optimal patch area. This effect can be regarded as the intrinsic coherence resonance [19,20]. In the presence of external periodic driving, the interspike interval histograms clearly demonstrate a synchronization of firing events with the external driving for large and intermediate patch sizes, while for small membrane patches the channel noise reigns the spiking dynamics. Due to the excitation of higher harmonics, a perfect frequency synchronization could not be observed. Instead, the Rice frequency, which is defined by the occurrence frequency of action potentials, exhibits a plateau-like structure for subthreshold signals: over a rather wide range of channel noise strength the Rice frequency can be fixed at a value smaller than the driving frequency. Furthermore, it was shown that the Hilbert frequency of the voltage signal equals to the Rice frequency of the spike process and, therefore, this average Rice frequency also reveals an imperfect synchronization behavior.

Acknowledgements

This work has been supported by the Deutsche Forschungsgemeinschaft via the Sonderforschungsbereich SFB-486, *Manipulation of matter on the nanoscale*, Project A10.

References

[1] A. Pikovsky, M. Rosenblum, J. Kurths, Synchronization: A Universal Concept in Nonlinear Sciences, Cambridge University Press, Cambridge, 2001.
[2] V. Anishchenko, A. Neiman, A. Astakhov, T. Vadiavasova, L. Schimansky-Geier, Chaotic and Stochastic Processes in Dynamic Systems, Springer, Berlin, 2002.
[3] J.A. Freund, L. Schimansky-Geier, P. Hänggi, Chaos 13 (2003) 225.
[4] W. Singer, Neuron 24 (1999) 49.
[5] E. Morse, Science 43 (1916) 169.
[6] C. Schäfer, M.G. Rosenblum, H.-H. Abel, J. Kurths, Phys. Rev. E 60 (1999) 857.
[7] A. Neiman, X. Pei, D. Russell, W. Wojtenek, l. Wilkens, F. Moss, H.A. Braun, M.T. Huber, K. Voigt, Phys. Rev. Lett. 82 (1999) 660.
[8] P. Tass, M.G. Rosenblum, J. Weule, J. Kurths, A. Pikovsky, J. Volkamnn, A. Schnitzler, H.-J. Freund, Phys. Rev. Lett. 81 (1998) 3291.
[9] J.A. Freund, A.B. Neiman, L. Schimansky-Geier, Europhys. Lett. 50 (2000) 8.
[10] D. Reguera, P. Reimann, P. Hänggi, J.M. Rubi, Europhys. Lett. 57 (2002) 644.
[11] L. Callenbach, P. Hänggi, S.J. Linz, J.A. Freund, L. Schimansky-Geier, Phys. Rev. E 65 (2002) 051110.
[12] M.G. Rosenblum, A.S. Pikovsky, J. Kurths, Phys. Rev. Lett. 76 (1996) 1804.
[13] A. Neiman, L. Schimansky-Geier, F. Moss, B. Shulgin, J.J. Collins, Phys. Rev. E 60 (1999) 284.
[14] A.L. Hodgkin, A.F. Huxley, J. Physiol. (London) 117 (1952) 500.
[15] B. Hille, Ionic Channels of Excitable Membranes, 2nd Edition, Sinauer Associates, Sunderland, MA, 1992.
[16] B. Sakmann, E. Neher, Single-Channel Recordings, Plenum Press, New York, 1995.

[17] J.A. White, J.T. Rubinstein, A.R. Kay, Trends Neurosci. 23 (2000) 131.
[18] J.R. Clay, L.J. DeFelice, Biophys. J. 42 (1983) 151;
A.F. Strassberg, L.J. DeFelice, Neural Comput. 5 (1993) 843;
L.J. DeFelice, A. Isaac, J. Stat. Phys. 70 (1993) 339.
[19] G. Schmid, I. Goychuk, P. Hänggi, Europhys. Lett. 56 (2001) 22.
[20] P. Jung, J.W. Shuai, Europhys. Lett. 56 (2001) 29.
[21] R.F. Fox, Y. Lu, Phys. Rev. E 49 (1994) 3421.
[22] D. Gabor, J. Inst. Electr. Eng. Part 3 93 (1946) 429.
[23] P. Panter, Modulation, Noise, and Spectral Analysis, McGraw-Hill, New York, 1965.
[24] S.O. Rice, Bell System Tech. J. 23/24 (1944) 1;
S.O. Rice, Bell System Tech. J. 23/24 (1994) 57.
[25] R. Toral, C. Masoller, C.R. Mirasso, M. Ciszak, O. Calvo, Physica A 325 (2003) 192 [these proceedings].